Data-driven analysis techniques for plasma space propulsion experiments and simulations

Mario Merino, Davide Maddaloni, Borja Bayón Buján, Filippo Terragni, Jaume Navarro-Cavallé

PLASMA 2023, September 18-22, 2023, Warsaw (Poland)

Contents

Motivation

- Data-driven analyses techniques do not replace, but complement, traditional approaches:
  - Extract additional insight from existing data
  - Automate data processing in a reproducible manner while reducing researcher bias
  - Process large and/or high-dimensional data
- Still not widely used in plasma propulsion
- In this talk we explore the application of 4 algorithms to process simulation and experimental data in plasma space propulsion:
  - POD
  - DMD
  - SINDy

  → Hall effect thruster breathing mode simulation data
  - CSD dispersion relation → Helicon plasma thruster azimuthal oscillation data

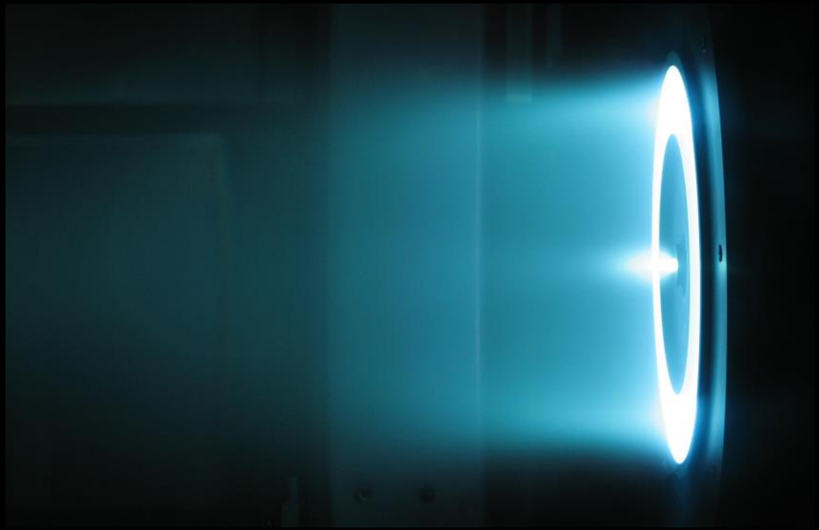

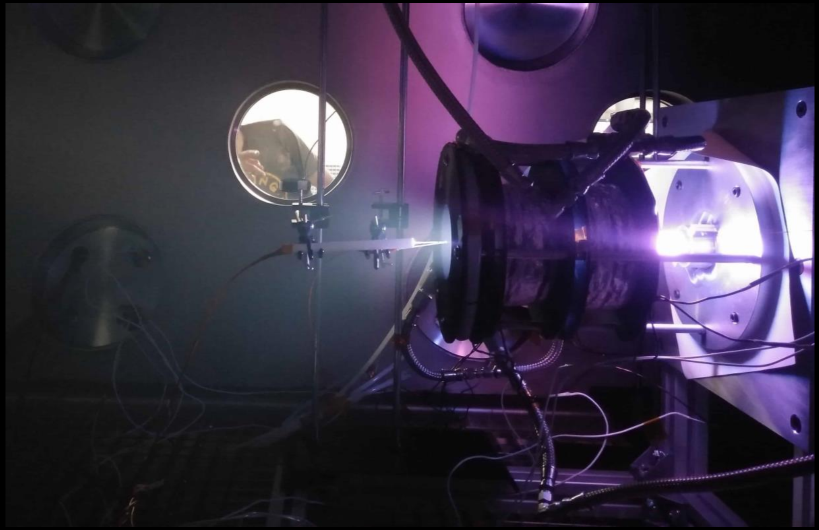

Overview of HET simulation data

- Axial-radial hybrid PIC/fluid code HYPHEN used to simulate the discharge of a SPT-100-like HET on Xe
  - Code developed, verified and validated over the last decade, building on previous experiences
  - Includes ionization, excitation, charge-exchange collisions and a tuned empirical model for anomalous transport
  - Discharge exhibits global oscillations (breathing mode) at 10-20 kHz, and traveling axial oscillations (ion transit mode) at 100-200 kHz
  - Discharge current oscillations (example below) correspond well with experimental observations:

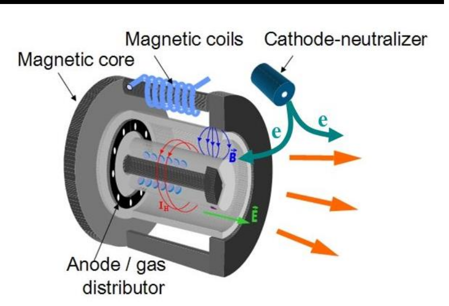

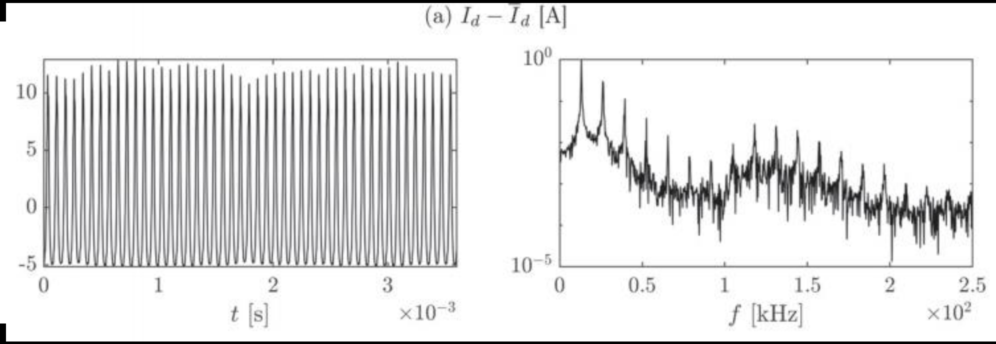

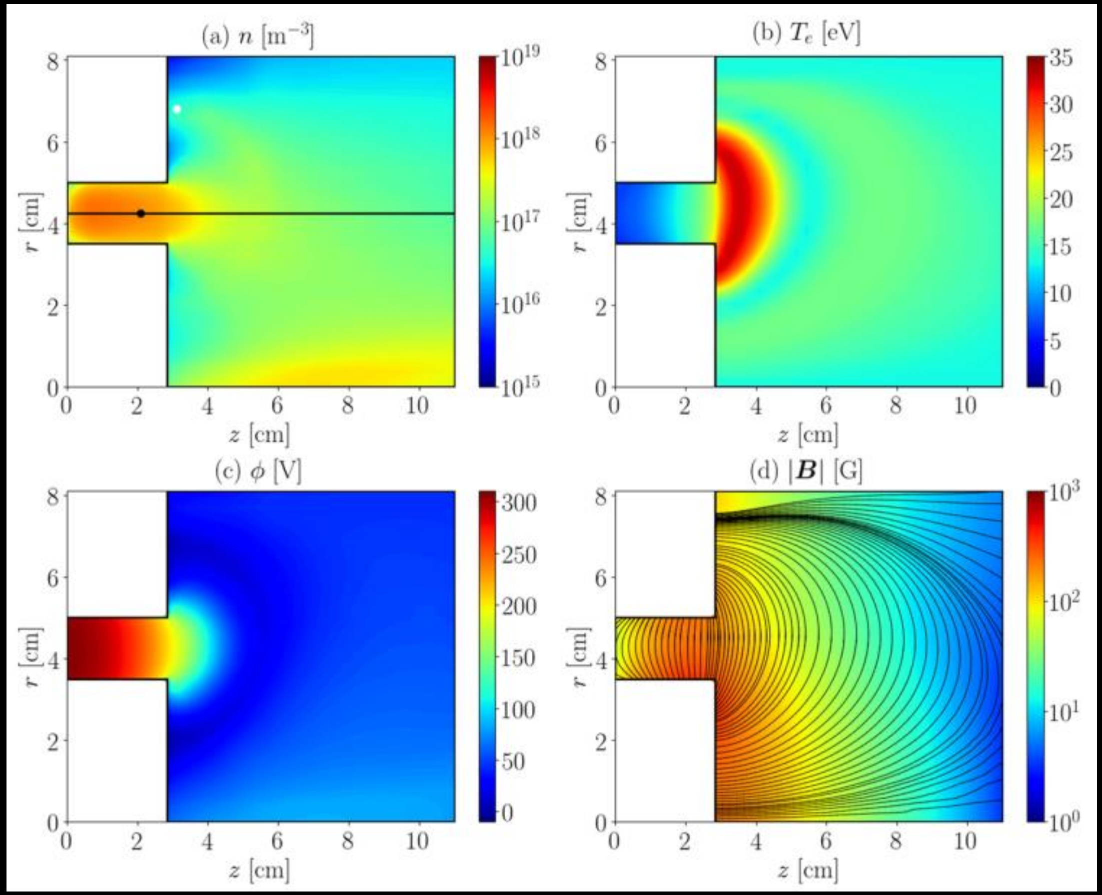

Nominal operating point:
$V_d = 300$ V
$\dot{m}_A = 5$ mg/s Xe

Proper orthogonal decomposition

- POD offers a quick first decomposition of the data into spatio-temporal modes, optimal according to an energy norm
  - “Most energy in less modes”
- All data (n, T_e, ϕ, etc) concatenated into a column vector $\boldsymbol{q}_n$ for each time instant, to form the snapshot matrix Q

$$\boldsymbol{Q} = [\boldsymbol{q}_1, \boldsymbol{q}_2, \ldots, \boldsymbol{q}_N]$$

- Standard SVD breaks Q into spatial modes W, temporal modes U, and singular value diagonal matrix Σ:

$$\boldsymbol{Q} = \boldsymbol{W}\boldsymbol{\Sigma}\boldsymbol{U}^{\mathrm{T}}$$

- POD modes do not separate according to frequency. BM and ITTM oscillations are mixed in some of the modes, and hence offers limited insight

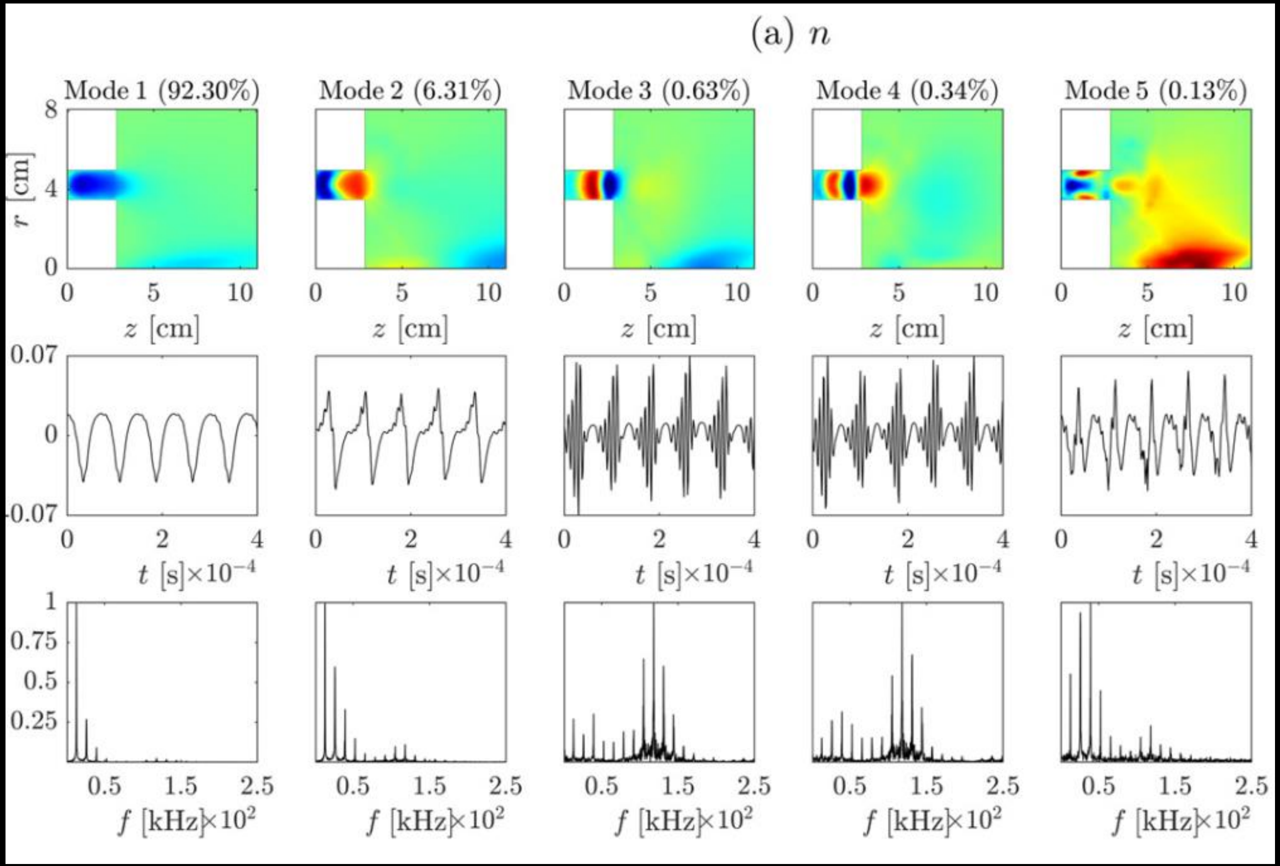

First 5 POD modes for plasma density in nominal case [Maddaloni et al 2022 PSST 31 045026]

High-order Dynamic mode decomposition

- Standard DMD seeks an expansion of $\boldsymbol{q}_n$ into spatial modes $\boldsymbol{\psi}_k$ and time exponentials $\exp[(\delta_k + i\omega_k)t_n]$:

$$\boldsymbol{q}_n \approx \boldsymbol{q}_n^{\mathrm{DMD}} = \sum_{k=1}^{K} a_k \boldsymbol{\psi}_k \, \mathrm{e}^{(\delta_k + \mathrm{i}\omega_k)t_n}$$

  - The dynamic relevance of a mode is given by its real amplitude a_k
- This is adequate to represent linear phenomena like oscillations and exponential growth/decay, whose evolution is given by Koopman matrix A:

$$\boldsymbol{q}_{n+1} = \boldsymbol{A}\boldsymbol{q}_n$$

- Higher-order DMD solves for:

$$\boldsymbol{q}_{n+d} = \boldsymbol{A}_1\boldsymbol{q}_n + \boldsymbol{A}_2\boldsymbol{q}_{n+1} + \cdots + \boldsymbol{A}_d\boldsymbol{q}_{n+d-1}$$

- Or equivalently:

$$\widetilde{\boldsymbol{q}}_{n+1} = \widetilde{\boldsymbol{A}}\widetilde{\boldsymbol{q}}_n$$

with:

$$\widetilde{\boldsymbol{q}}_n = \begin{bmatrix} \boldsymbol{q}_n \\ \boldsymbol{q}_{n+1} \\ \vdots \\ \boldsymbol{q}_{n+d-2} \\ \boldsymbol{q}_{n+d-1} \end{bmatrix}$$

$$\widetilde{\boldsymbol{A}} = \begin{bmatrix} \boldsymbol{0} & \boldsymbol{I} & \boldsymbol{0} & \dots & \boldsymbol{0} & \boldsymbol{0} \\ \boldsymbol{0} & \boldsymbol{0} & \boldsymbol{I} & \dots & \boldsymbol{0} & \boldsymbol{0} \\ \vdots & \vdots & \vdots & \vdots & \vdots & \vdots \\ \boldsymbol{0} & \boldsymbol{0} & \boldsymbol{0} & \dots & \boldsymbol{I} & \boldsymbol{0} \\ \boldsymbol{A}_1 & \boldsymbol{A}_2 & \boldsymbol{A}_3 & \dots & \boldsymbol{A}_{d-1} & \boldsymbol{A}_d \end{bmatrix}$$

High-order Dynamic mode decomposition

- The procedure followed is that of [Le Clainche S et al 2017 J. Appl. Dyn. Syst. 16 882–925]. In essence:
  - Apply SVD filter on the original snapshot matrix Q
  - Build $\widetilde{Q}$ based on reconstructed Q^*
  - Standard DMD is applied to $\widetilde{Q}$ to obtain δ_k, ω_k
  - Least squares are used to compute a_k
- All mode amplitudes and growth rates:

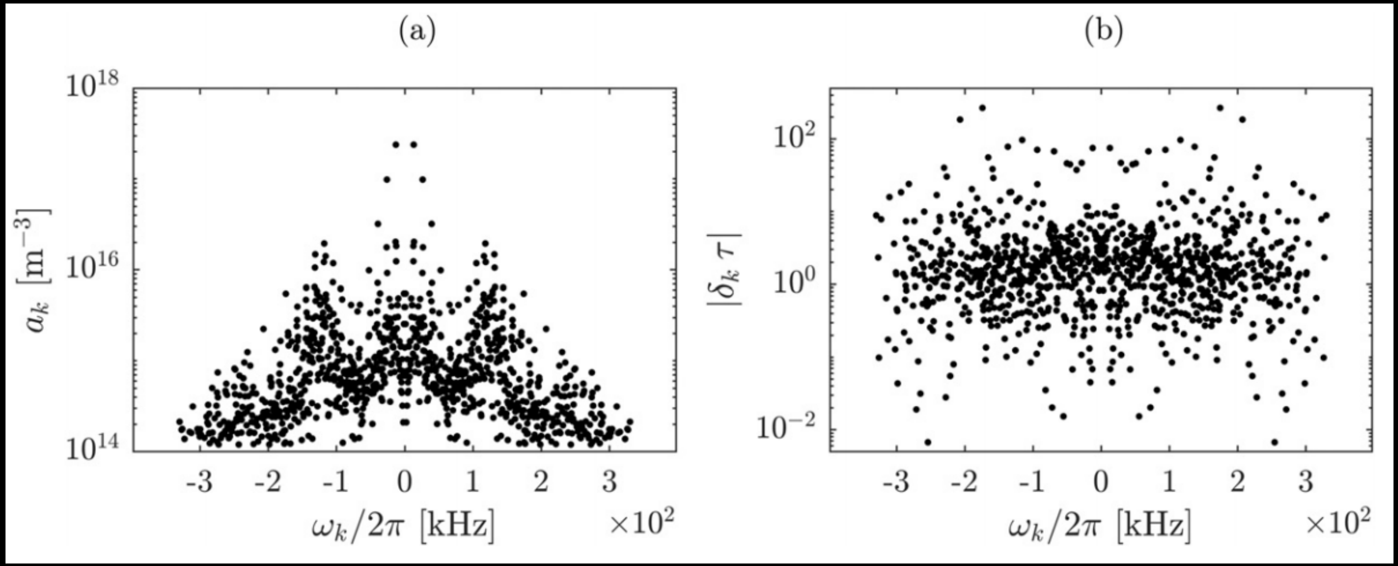

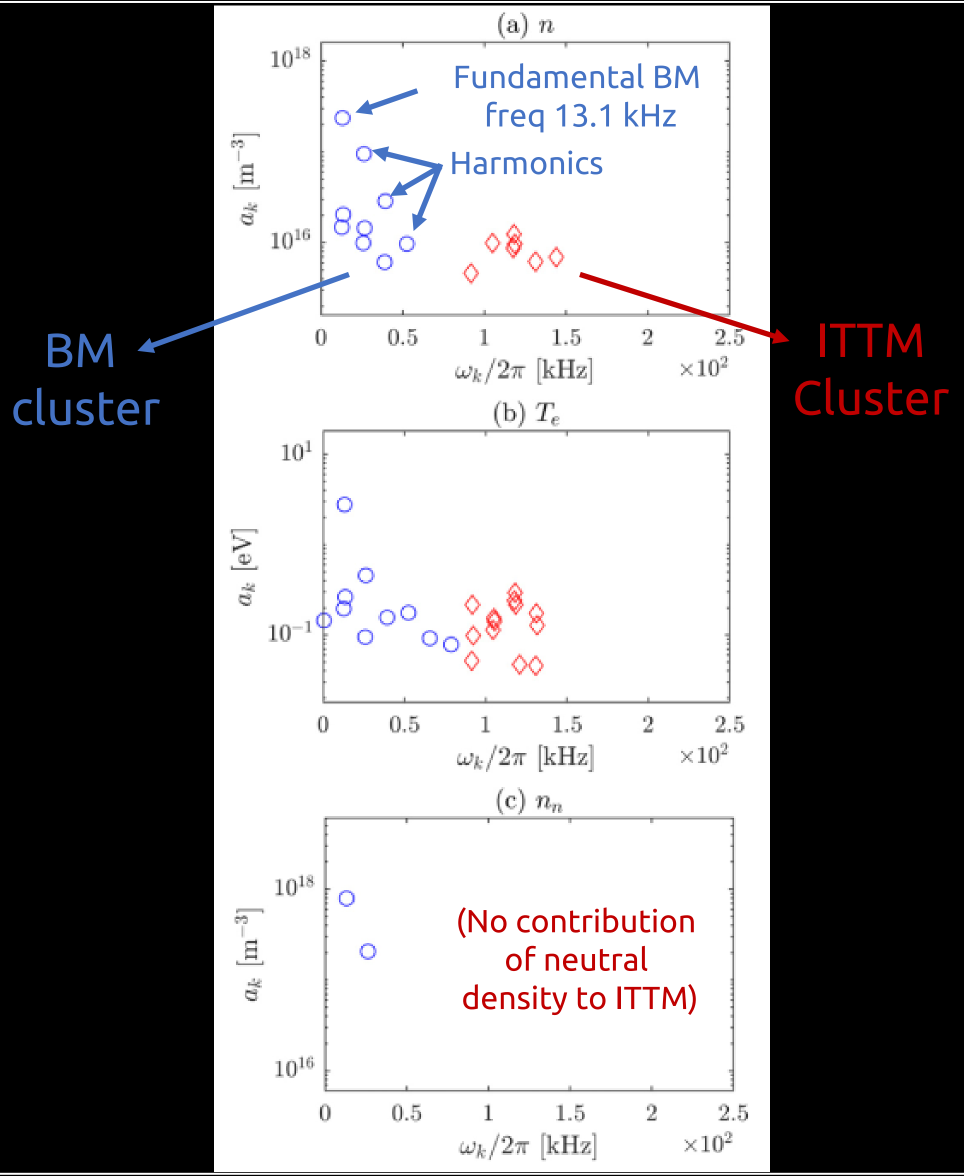

High-order Dynamic mode decomposition

- HODMD enables isolating BM and ITTM, and separating transcients from steady state oscillations:

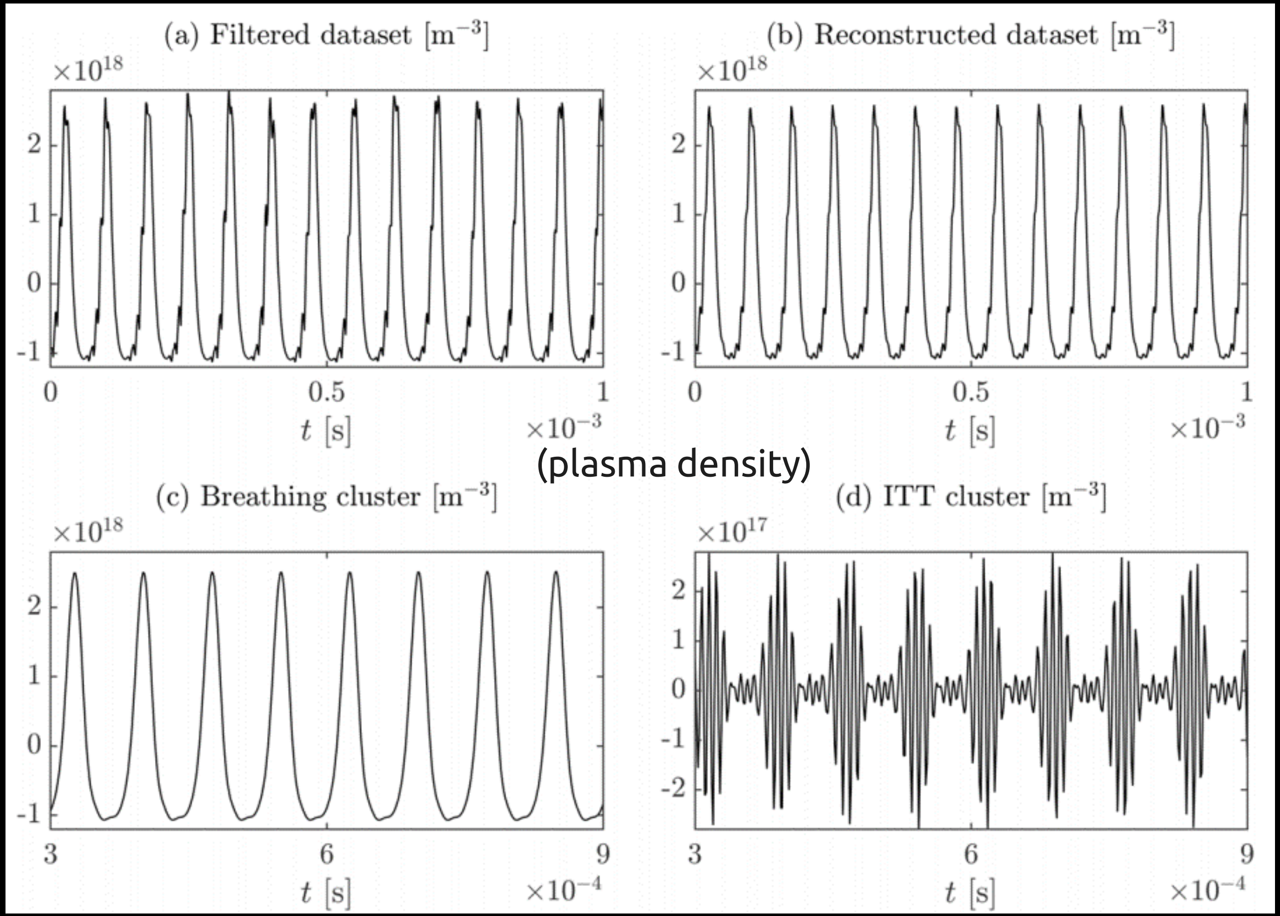

(plasma density)

Magnitude and phase of dominant BM component:

- Global oscillation of n, n_n
- Traveling oscillation of T_e, ϕ

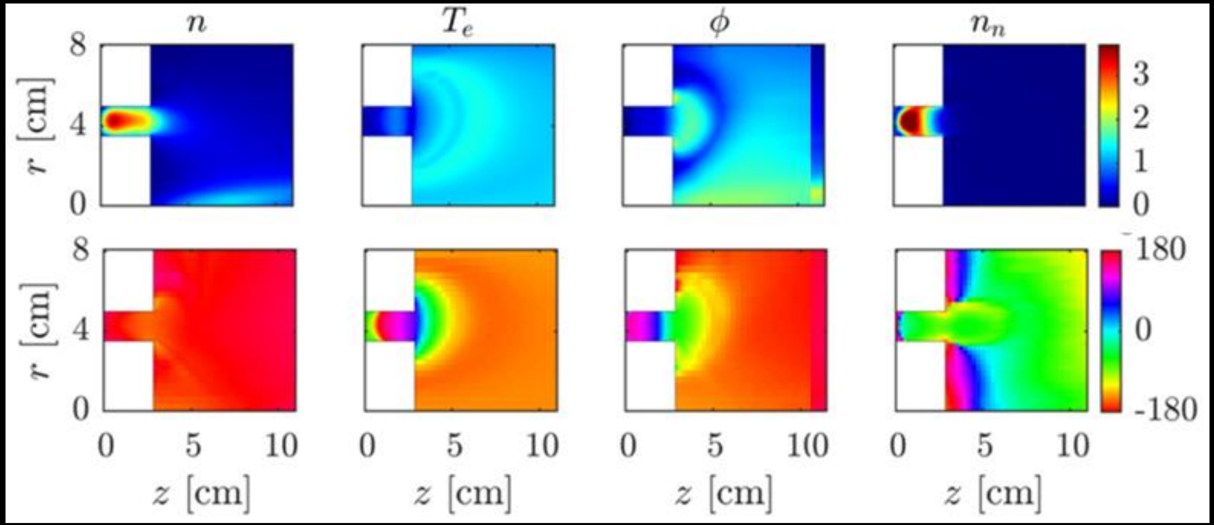

Breathing mode reconstruction (all variables)

High-order Dynamic mode decomposition

- ITTM consists instead of an essentially traveling wave in the axial direction:

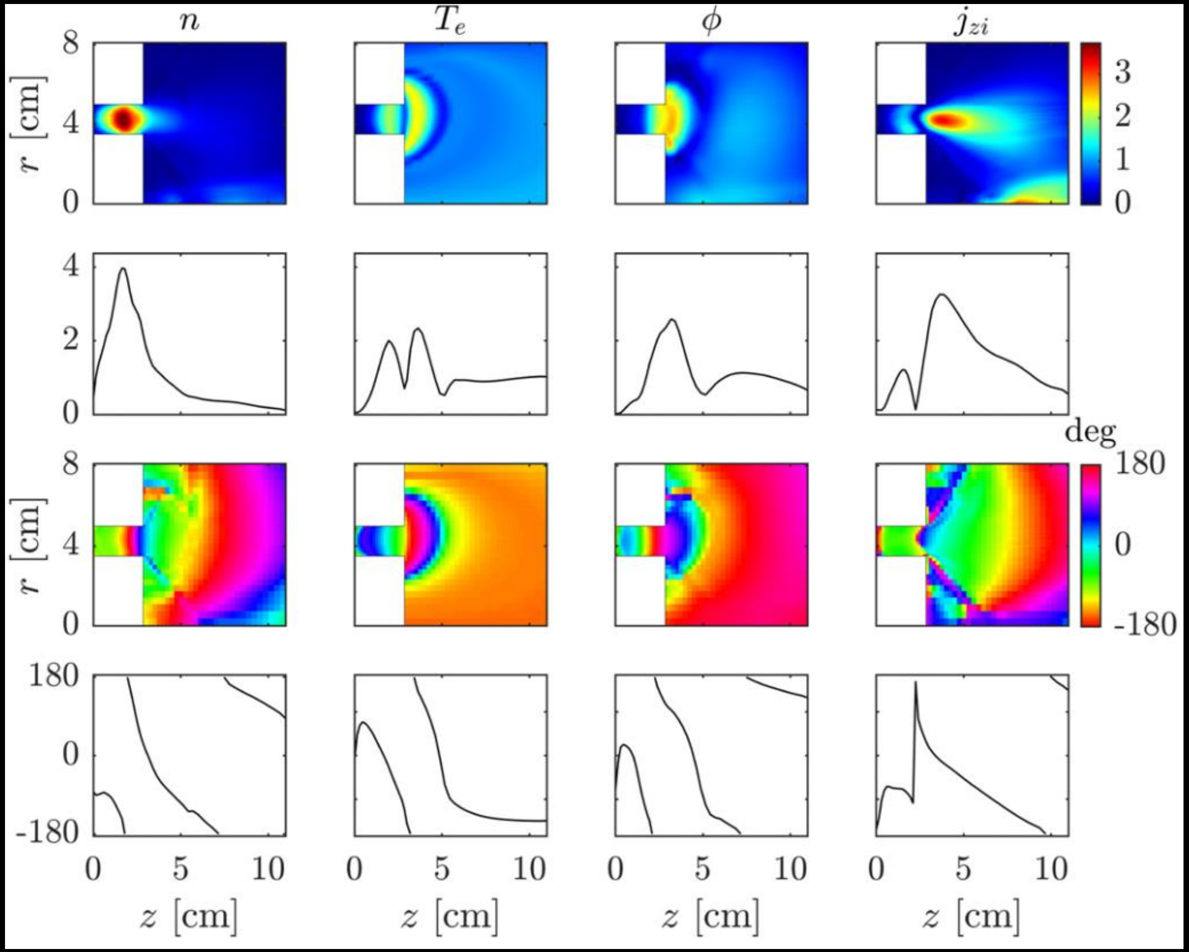

- 4 Snapshots of an ITTM cycle (reconstructed data):

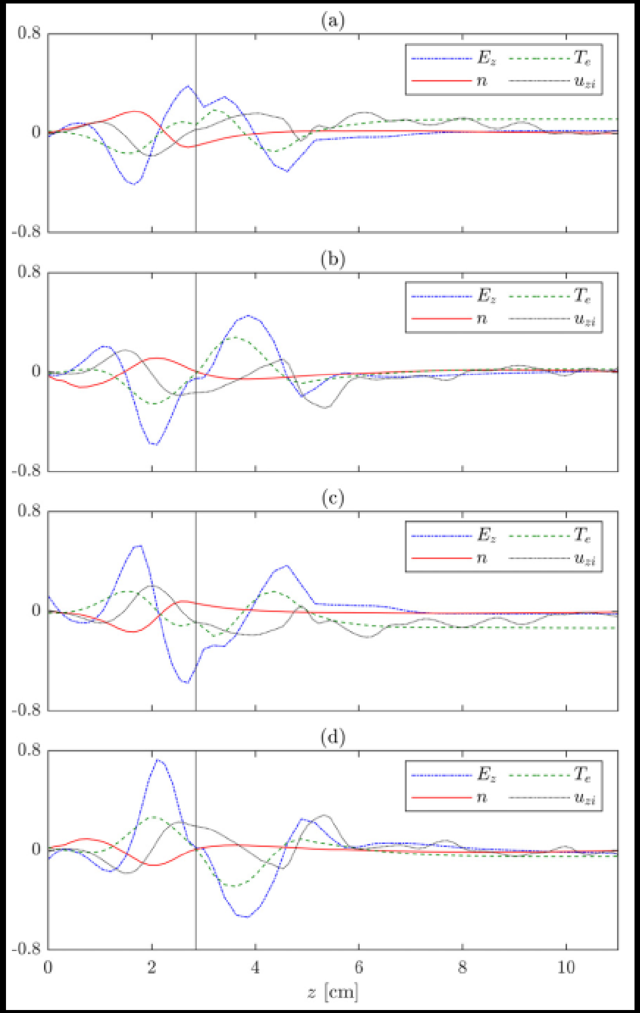

Symbolic Regression (SINDy)

- We now try to obtain the BM dynamic equations in the form:

$$\dot{n} = \beta_{11} n + \beta_{12} n_n + \beta_{13} T_e + \beta_{14} n^2 + \cdots$$
$$\dot{n}_n = \beta_{21} n + \beta_{22} n_n + \beta_{23} T_e + \beta_{24} n^2 + \cdots$$
$$\ldots$$

or, more generally, for a prescribed function library Θ_j:

$$\dot{\hat{x}}_{ik} = \beta_{ij} \Theta_j(\hat{\boldsymbol{x}}(t_k), t_k)$$

- We use the data to numerically estimate the derivatives on the left hand side, and then least squares to minimize the error $\varepsilon = \varepsilon^S + \lambda \varepsilon^\lambda$, with:

$$\varepsilon^S = \sum_{i,k} \left\| \dot{\hat{x}}_{ik} - \beta_{ij} \hat{\Theta}_{jk} \right\|^2 \qquad \varepsilon^\lambda = |a_{ij} \beta_{ij}|$$

  - $\lambda \varepsilon^\lambda$ is a sparsity-promoting term that penalizes near-zero β_{ij} coefficients

- The Weak SINDy variant uses the weak form of the equation and replaces ε^S with the error:

$$\varepsilon^W = \sum_m \left\| \hat{x}_i(t_0^m) - \hat{x}_i(t_f^m) + \beta_{ij} \hat{\Theta}_{jk} w_j \right\|^2$$

- It is possible to apply e.g. linear constraints to the coefficients to exploit our physical knowledge of the system:

$$\beta_{ij} = C_{ijl} b_l$$

- Relevant to our analysis is also the integration error ε^I, which measures how well the numerically-integrated model equations reproduce the data:

$$\varepsilon^I = \sum_{i,k,p} \| \hat{x}_{ik}^p - \tilde{x}_{ik}^p \|^2$$

Global analysis

- We first try to extract dynamic equations for the average plasma properties in the indicated domain
- We vary the sparsity penalty λ and evaluate different models, selecting the knee of the pareto front

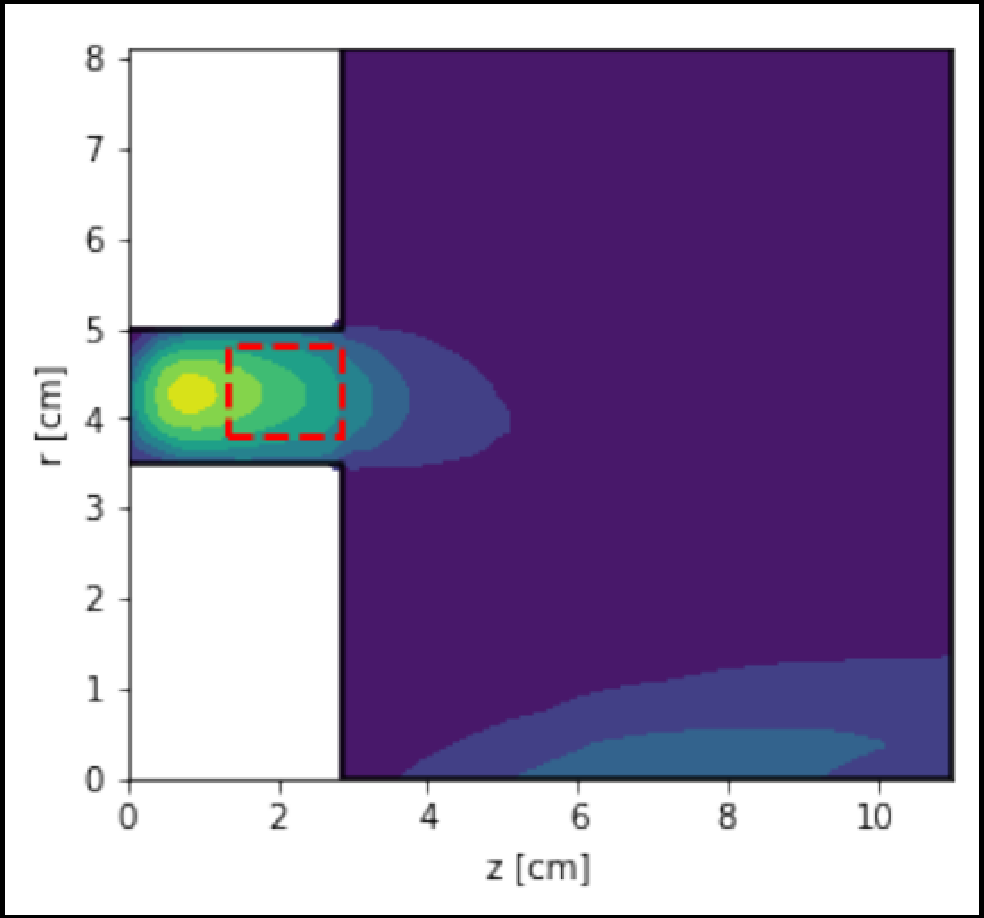

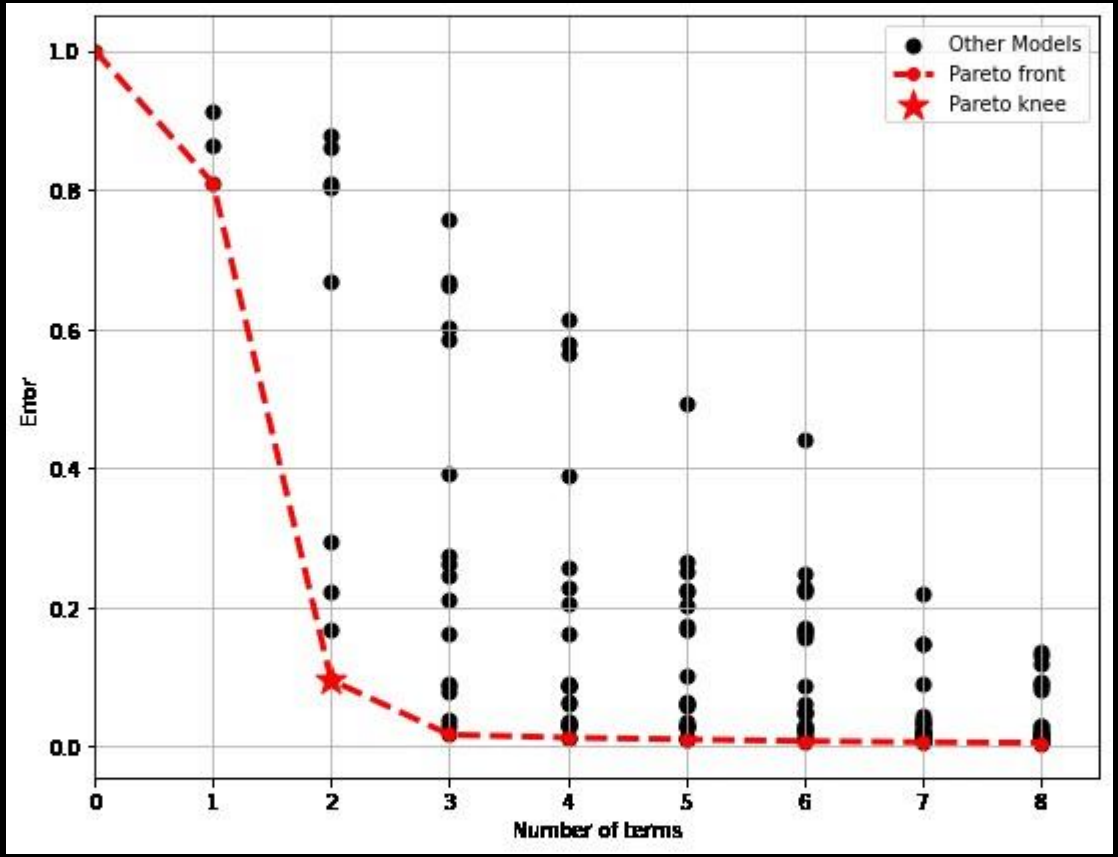

Global analysis

- Varing the breadth of the search library of functions we can search for models of varying complexity and detail, while still retaining physical interpretability
- The algorithm strives to match the derivative of each variable (e.g., the ion density:)

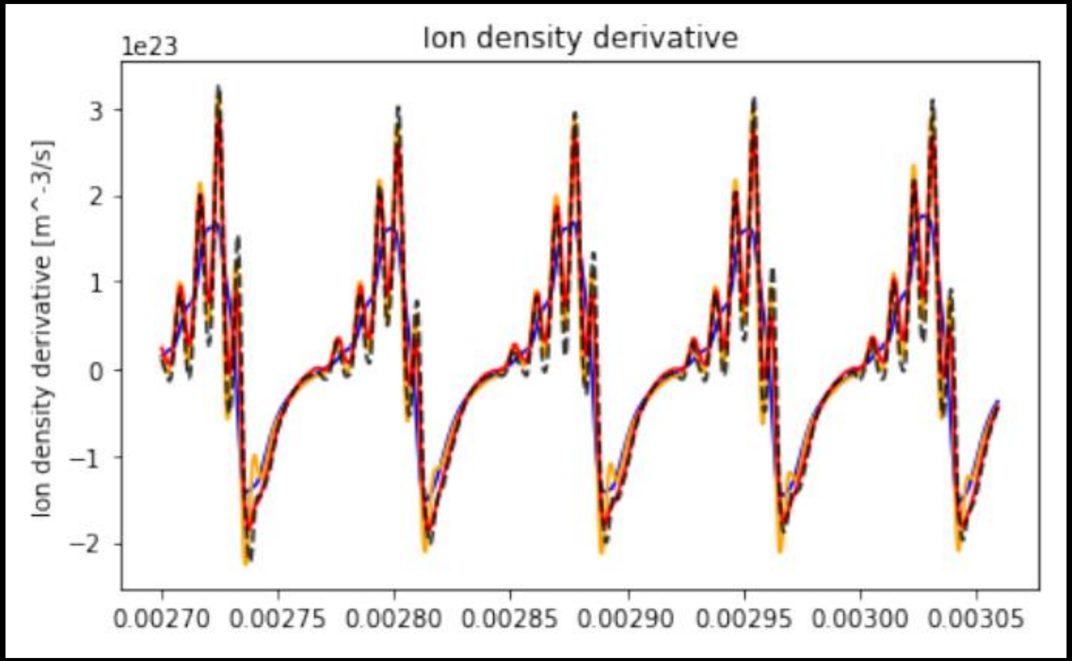

Including only n_n_n functions in the library:

$$\dot{n}_i = -1.45 \cdot 10^5 n_i + 4.12 \cdot 10^{-14} n_i n_n$$
$$\dot{n}_n = 4.58 \cdot 10^4 n_n - 4.89 \cdot 10^{-14} n_i n_n$$

Adding ionization rate $R_{ion}(T_e)$:

$$\dot{n}_i = -2.66 \cdot 10^5 n_i + 1.16\, n_i n_n R_{ion}$$
$$\dot{n}_n = 1.83 \cdot 10^{23} - 0.77\, n_i n_n R_{ion}$$

Adding axial velocity:

$$\dot{n}_i = -41.2\, n_i u_{i,z} + 0.82\, n_i n_n R_{ion}$$
$$\dot{n}_n = 1.83 \cdot 10^{23} - 0.77\, n_i n_n R_{ion}$$

- Best-fit equations found for T_e, u_{zi} are less interpretable:

$$\dot{T}_e = -2.30 \cdot 10^6 - 1.51 \cdot 10^{-12} n_n + +4.42 \cdot 10^{-16} n_n u_{i,z} + 5.99 \cdot 10^{-18} n_n u_{i,z} T_e$$
$$\dot{u}_{i,z} = 2.45 \cdot 10^5 u_{i,z} - 3.01 \cdot 10^6 T_e^2 - 1.81 \cdot 10^{-15} n_n u_{i,z} T_e$$

Global analysis

- How well the numerical integration of the model describes the data does not follow directly from the quality of the fit in the derivatives:
  - In this particular case, more complex models start to introduce spurious higher-frequency oscillations and a decaying behavior

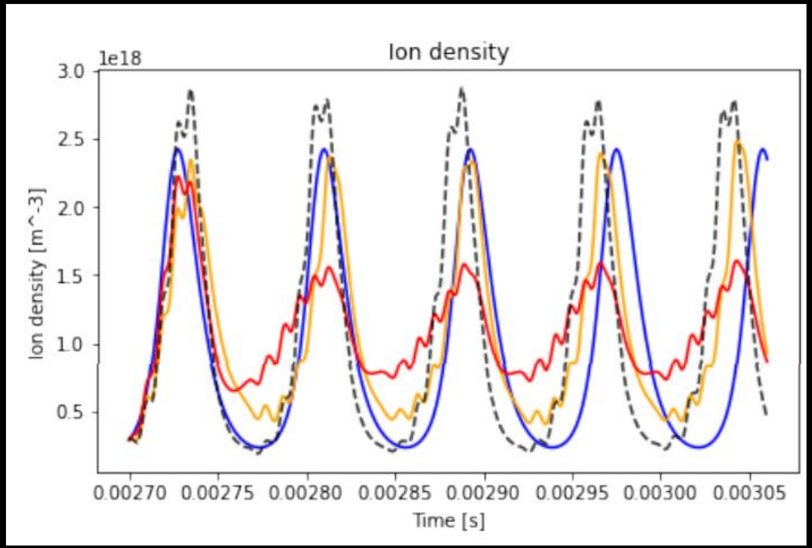

- Alternatively to ε^S we can minimize ε^W or ε^I, and/or apply the constraint that the magnitude of the ionization term be equal in the ion and neutral equations:

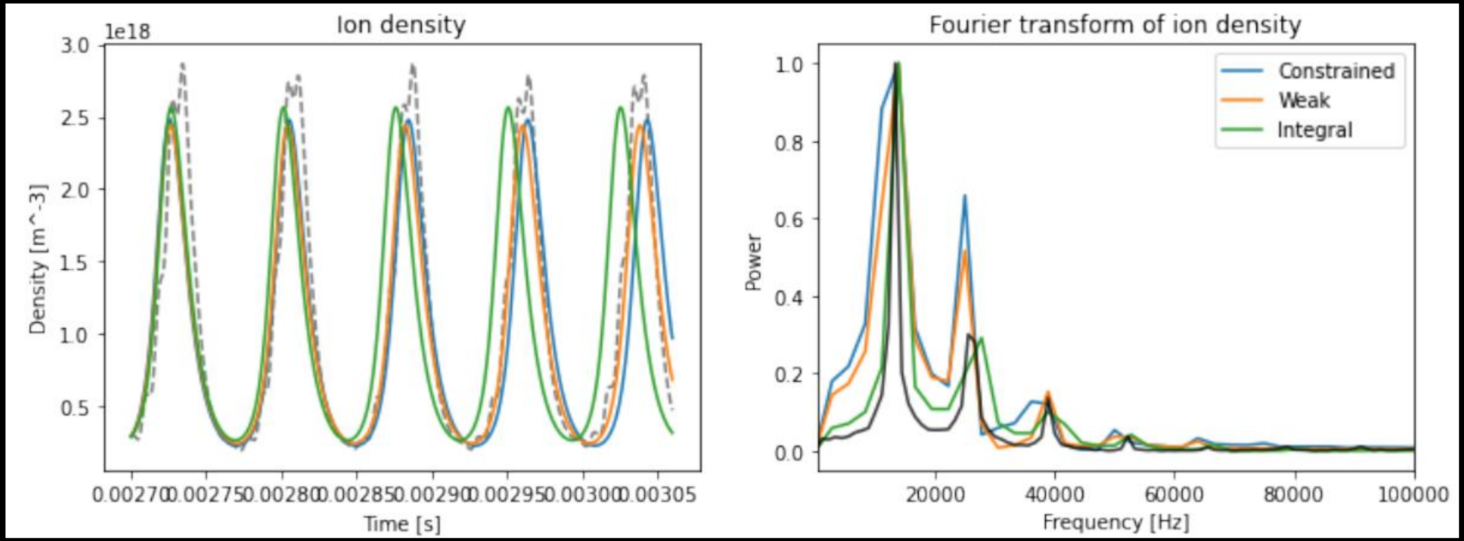

Global analysis

$$\dot{n}_i = n_i u_{i,z}/L + \epsilon_{ion,n_i}\, n_i n_n R_{ion}$$
$$\dot{n}_n = g_{inj} - \epsilon_{ion,n_n}\, n_i n_n R_{ion}$$

- Applying the same procedure at varying operating points we can find trends of the coefficients and fit simple laws:
- Increasing $\dot{m}_A$:
  - L increases slightly, suggesting a larger effective volume is involved in the BM oscillations
  - g_{inj} is proportional to $\dot{m}_A$ (consistency)
  - Ionization term decreases slightly but remains $\simeq 1$

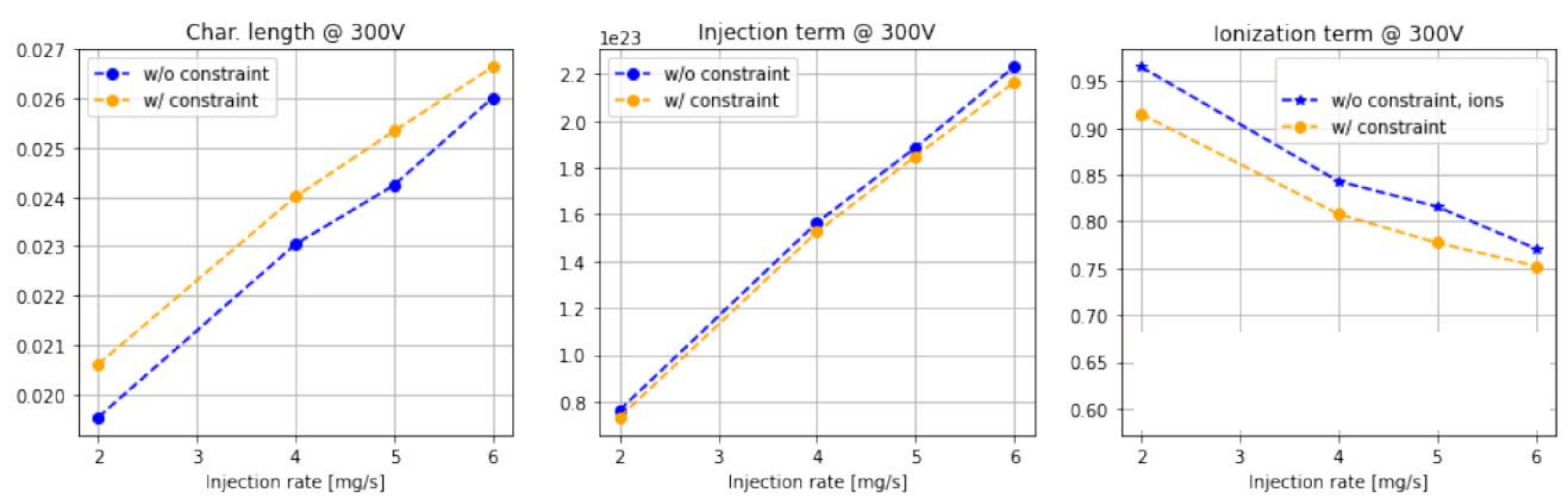

$V_D(V)$	$\dot{m}_A$ (mg/s)	L (cm)	$g_{inj}(m^{-3}/s)$	ϵ_{ion,n_i}
200	5	0.018	$2.36 \cdot 10^{23}$	1.06
300	2	0.020	$7.62 \cdot 10^{22}$	0.97
300	4	0.023	$1.56 \cdot 10^{23}$	0.84
300	5	0.024	$1.89 \cdot 10^{23}$	0.82
300	6	0.026	$2.23 \cdot 10^{23}$	0.77
400	5	0.026	$1.70 \cdot 10^{23}$	0.84

Point-wise analysis

- Finally, we can do the SINDy analysis for the plasma variables *at each point*, rather than their volume averages
- Presence (and magnitude) of the various coefficients helps separate different regions of the dicharge channel: rear, lateral walls; upstream region; downstream region

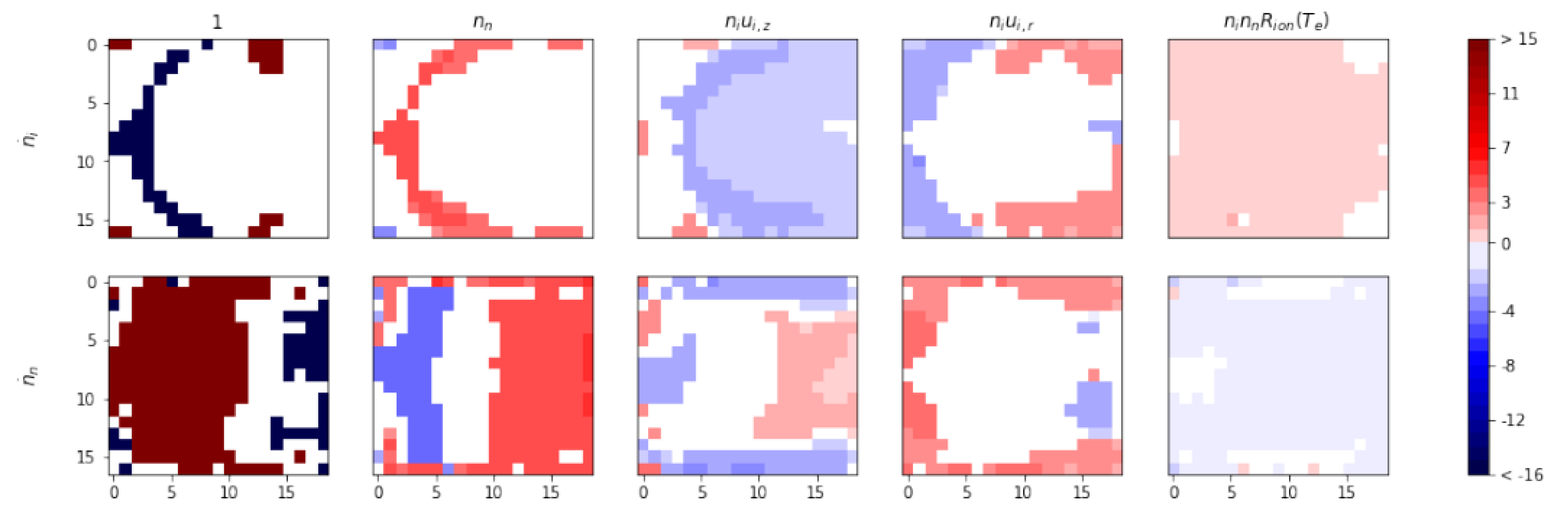

Contents

Azimuthal oscillations in a magnetic nozzle

- Helicon plasma thruster consists of
  - cylindrical dielectric ionization chamber
  - EM inductor (“antenna”)
  - Converging-diverging applied B field → Magnetic nozzle

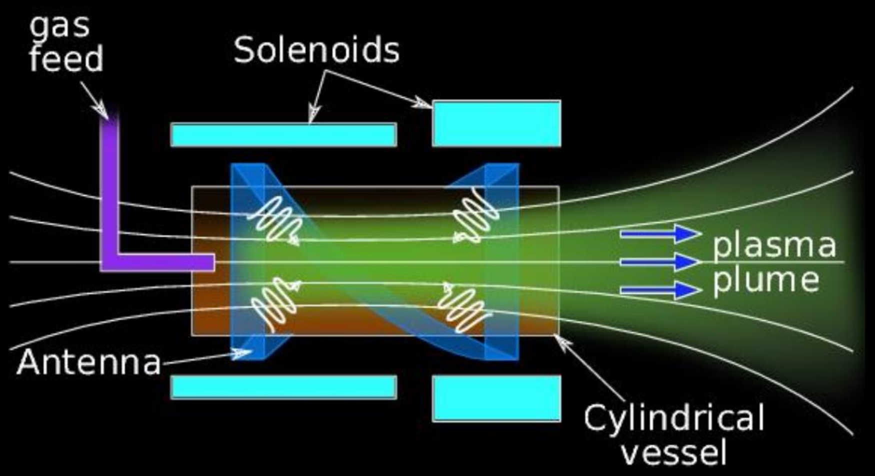

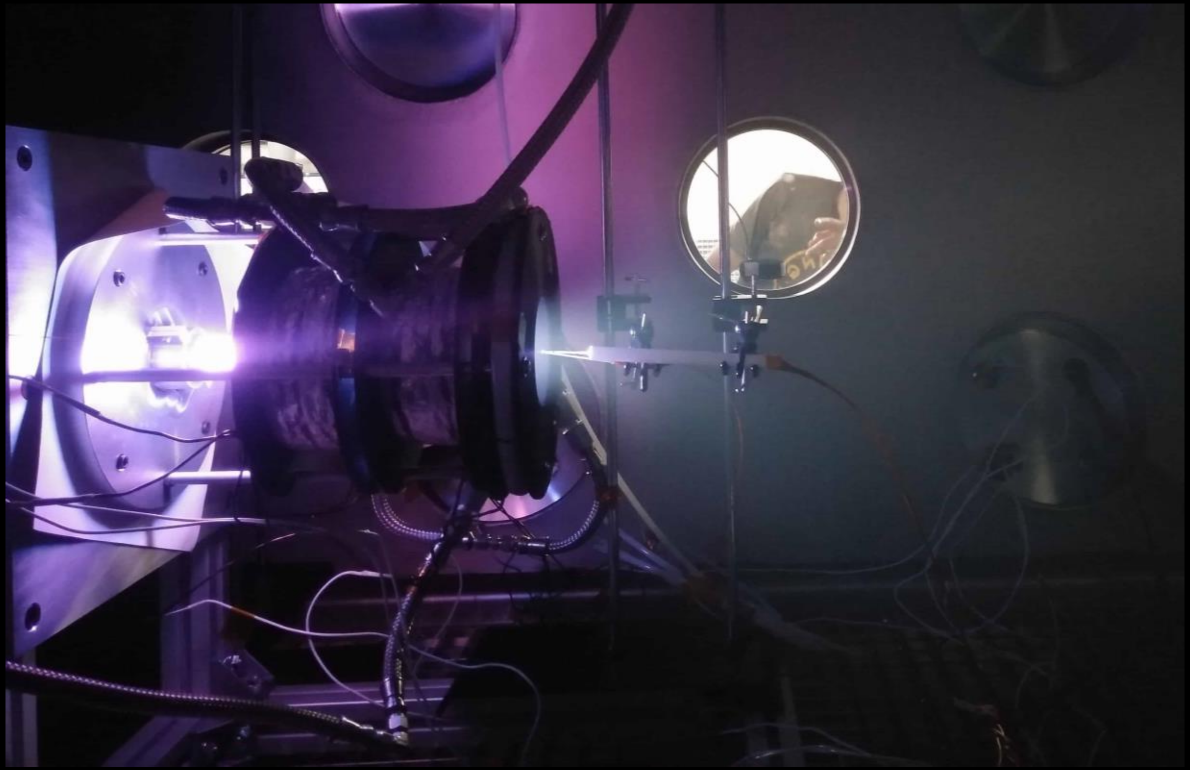

- Losses to lateral walls are large and suggest anomalous transport
- Gradient-driven drift instabilities are a candidate mechanism for that enhanced transport
- Previous works identify oscillations in the magnetic nozzle plasma plume

Experimental setup

- HPT prototype running at 5, 10, 20 sccm Xe, 450 W EM power
- Max. B field 750 G
- Vacuum chamber: 1.5 m diameter, 3.5 m length, 10^{-5} mbar during operation
- 3 floating, cylindrical tungsten probe tips, 1 cm apart (along θ and d directions)
- Probe system displaced with radial-polar arm to desired locations

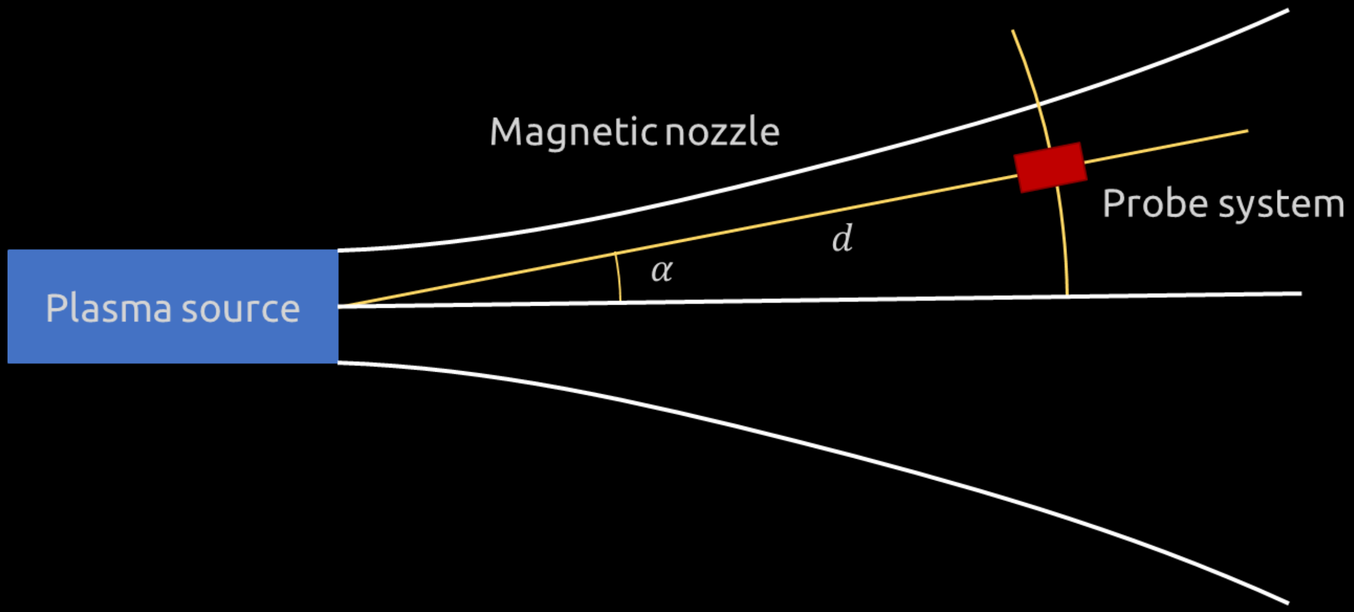

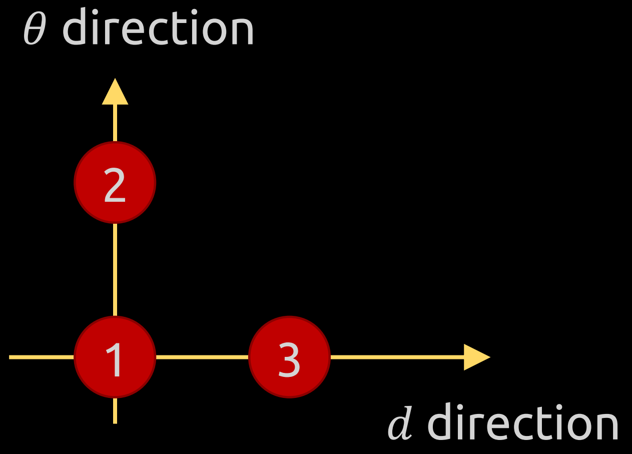

Cross correlation analysis

- 30 realizations of the cross correlation spectrum between 2 probes:

$$C(\omega) = X_2(\omega) X_1^*(\omega)$$

- Mean and deviation of log power $c = \log C$:

$$\bar{\mu}_c = \frac{1}{n}\sum_k^n c_k \qquad \bar{\sigma}_c = \sqrt{\frac{1}{n-1}\sum_k^n (c_k - \bar{\mu}_c)^2}$$

- Mean and deviation phase difference (circular statistics):

$$\tilde{\mu}_\phi = \arg \tilde{z}$$

$$\tilde{z} = \frac{1}{n}\sum_k^n \exp(i\phi_k) \qquad d_1 = \frac{1}{n}\sum_k^n |\phi_k - \mu_{\tilde{\phi}}|$$

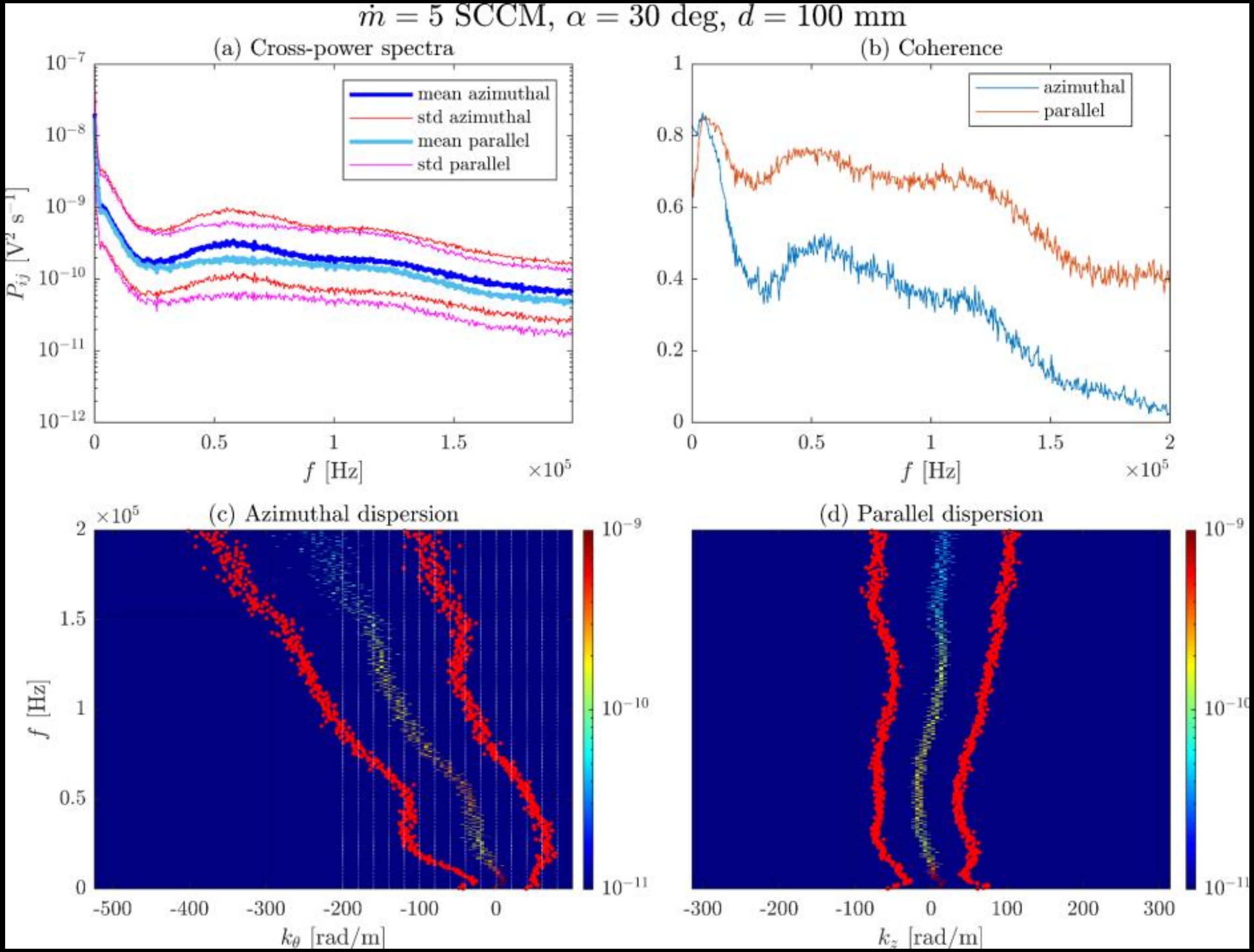

Cross correlation analysis

- Example at one location ($d = 100$ mm, $\alpha = 30$ deg)
- Peak in CSD power and coherence at ~60 kHz
  - Harmonic at ~120 kHz suggests nonlinear effects present
  - Flatter spectrum found at $d = 150$ mm
- Azimuthal dispersion compatible with gradient drift and ExB drift estimated velocities ($1\text{-}4 \cdot 10^4$ m/s)
  - This is only found at intermediate α angles
- Parallel dispersion relation is $k_z \simeq 0$
- Oscillations die out as mass flow rate is increased
- Various candidate oscillations/instabilities
  - Drift waves are a good candidate

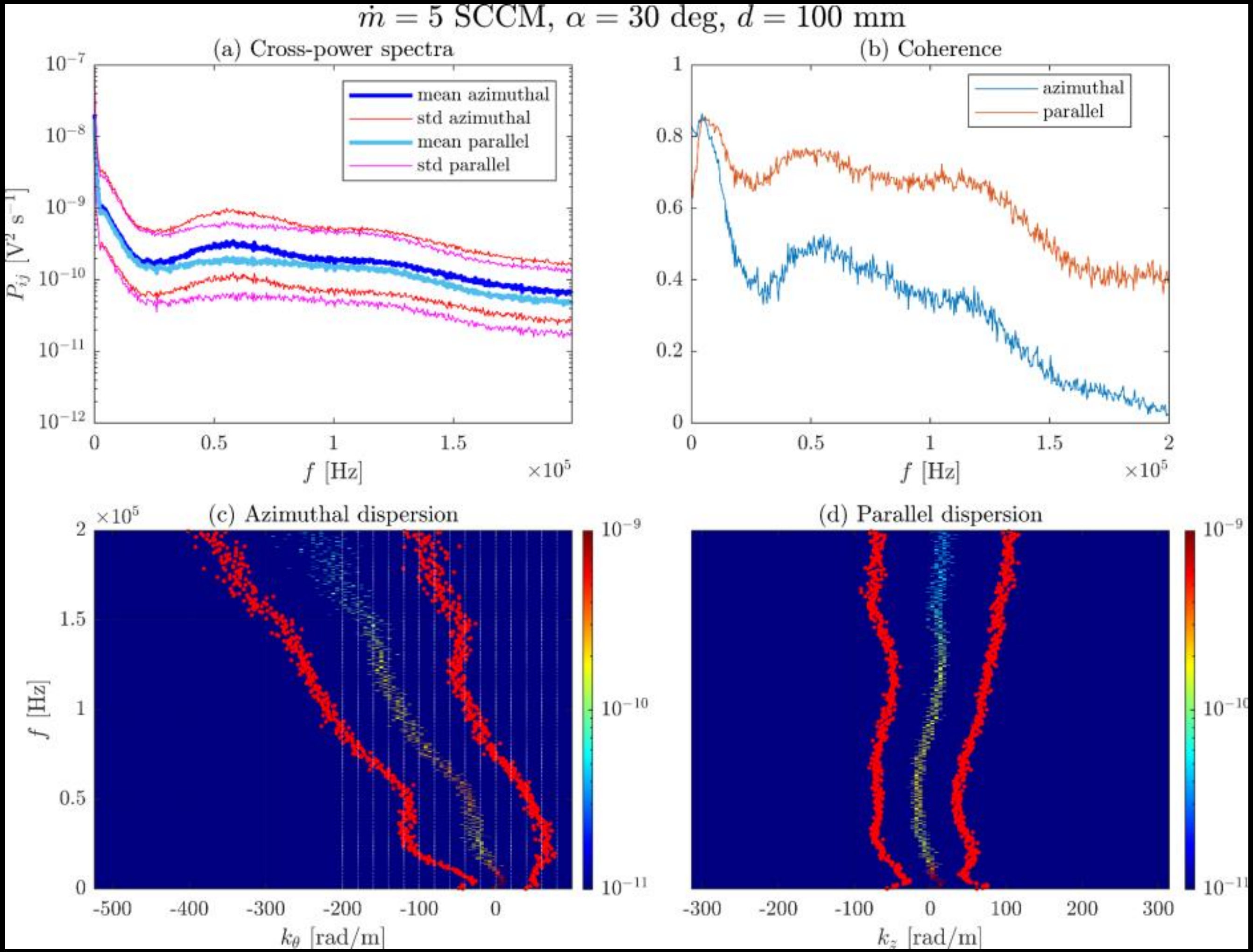

Dispersion relation discussion

- Other works (below) also found azimuthal oscillations in similar setups
  - Hepner et al: suggest ECDI
  - Takahashi: suggests oscillations are a magnetosonic wave
- Further work (experimental and theoretical) needed to clarify nature of oscillations and role on transport+

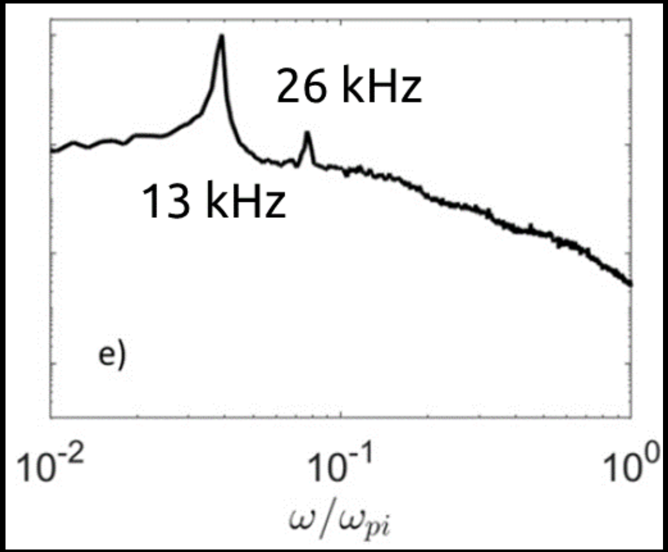

Hepner et al ECRT
Appl. Phys. Lett. 116, 263502 (2020);
Proposes outward electron transport

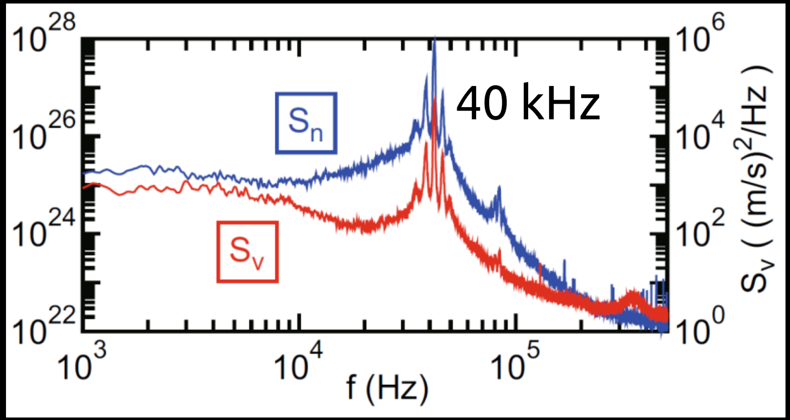

Takahashi's HPT
Scientific Reports (2022) 12:20137;
Proposes inward electron transport

Contents

Summary and way forward

- Data-driven analysis techniques can be (partially?) useful tools to interpret simulation and experimental results. We have explored a tiny subset of techniques and applied them to HET BM and MN azimuthal oscillation analysis
- Linear techniques like POD, (HO)DMD useful at decomposing data in different spatio-temporal bases, helping isolate modes of interest
    - Best-suited technique depends strongly on data and research objectives
- Symbolic regression (SINDy) is great to identify simple, (interpretable?) models behind the data. Method is amenable to applying prior physical knowledge of the system
    - In our analysis of BM oscillations, including spatial gradients of the variables in the SINDy search library and allowing for higher-order differential equations would lead to PDEs describing the time and space dynamics
- Cross correlation analysis among probes can help resolve dispersion relation of MN oscillations. This topic is still at a preliminary stage
    - Understanding which oscillation/instabilities manifest requires additional data and further theoretical work
    - Adding additional probes may help resolve the full 3D $\boldsymbol{k}$ vector of the oscillation and disambiguate multiple waves at a given frequency

Acknowledgments

This project has received funding from the European Research Council (ERC) under the European Union's Horizon 2020 research and innovation programme (grant agreement No 950466)

Thank you!

mario.merino@uc3m.es

ZARATHUSTRA

EP2 uc3m

erc

Table 1. Main SPT-100-like HET simulation parameters for the nominal and off-nominal cases, together with the peak values of the time-averaged maps of the main variables. Refer to [37] for further details regarding the simulation parameters that are not mentioned here.

Simulation parameter / variable peak	Units	Nominal case	Low voltage case	High mass flow rate case
PIC mesh number of cells, nodes	—	1464, 1553		
MFAM number of cells, faces	—	4822, 9796		
Cathode location: z, r	cm	3.12, 6.80		
Simulation (PIC) timestep, Δt	$\mathrm{s} \times 10^{-8}$	1.50		
Total number of simulation steps	—	240 000		
Injected Xe mass flow, $\dot{m}_A$	$\mathrm{mg\ s^{-1}}$	5	5	6
Discharge voltage, V_d	V	300	200	300
Average discharge power, P_d	kW	1.8	1.0	2.2
Plasma density, n	$\mathrm{m^{-3}} \times 10^{18}$	1.50	1.43	1.84
Electron temperature, T_e	eV	32.8	22.7	32.9
Total axial ion current density, j_{zi}	$\mathrm{A\ m^{-2}} \times 10^{3}$	1.17	1.08	1.44
Neutral density, n_n	$\mathrm{m^{-3}} \times 10^{19}$	2.88	2.90	3.47